

Mamba-Based Modality Disentanglement Network for Multi-Contrast MRI Reconstruction

Weiye Lyu, Xinming Fang, Jun Wang, Jun Shi, Guixu Zhang, Juncheng Li*

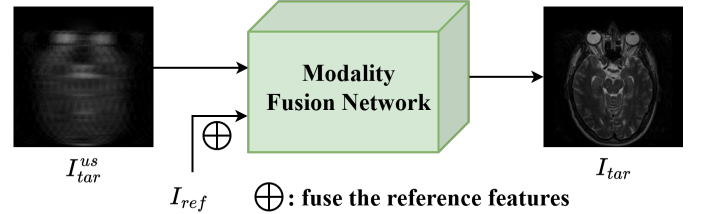
Abstract—Magnetic resonance imaging (MRI) is a cornerstone of modern clinical diagnosis, offering unparalleled soft-tissue contrast without ionizing radiation. However, prolonged scan times remain a major barrier to patient throughput and comfort. Existing accelerated MRI techniques often struggle with two key challenges: (1) failure to effectively utilize inherent K-space prior information, leading to persistent aliasing artifacts from zero-filled inputs; and (2) contamination of target reconstruction quality by irrelevant information when employing multi-contrast fusion strategies. To overcome these challenges, we present MambaMDN, a dual-domain framework for multi-contrast MRI reconstruction. Our approach first employs fully-sampled reference K-space data to complete the undersampled target data, generating structurally aligned but modality-mixed inputs. Subsequently, we develop a Mamba-based modality disentanglement network to extract and remove reference-specific features from the mixed representation. Furthermore, we introduce an iterative refinement mechanism to progressively enhance reconstruction accuracy through repeated feature purification. Extensive experiments demonstrate that MambaMDN can significantly outperform existing multi-contrast reconstruction methods.

Index Terms—Multi-contrast MRI reconstruction, dual-domain learning, Mamba, modality disentanglement

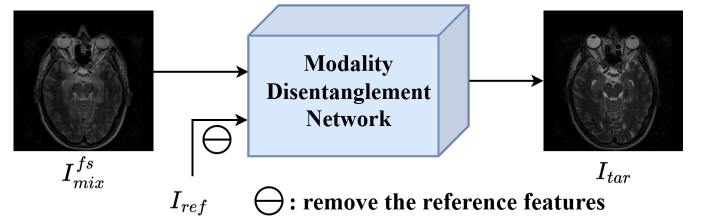
I. INTRODUCTION

MAGNETIC resonance imaging (MRI) is a vital diagnostic tool, providing unparalleled soft-tissue contrast without ionizing radiation—making it indispensable for neurological, musculoskeletal, and oncological imaging. Unlike Computed Tomography (CT), X-ray, or Positron Emission Tomography (PET), MRI avoids radiation exposure, enabling safer repeated scans for chronic disease monitoring and pediatric cases. However, its widespread clinical utility is hampered by three fundamental limitations, including 1) K-space sampling constraints, 2) multi-sequence protocols, and 3) physically limited timing. These factors contribute to patient discomfort, motion artifacts, and reduced clinical throughput, particularly serious in resource-limited healthcare settings.

Fast MRI reconstruction techniques address a critical clinical need by enabling high-quality image recovery from under-sampled k-space data, significantly reducing acquisition times while maintaining diagnostic utility. Traditional approaches, such as Parallel Imaging (PI) [1], [2] and Compressed Sensing (CS) [3], leverage the sparsity of transformed domains and incorporate prior information into regularized optimization frameworks. These methods also exploit the redundancy



(a) Multi-contrast MRI reconstruction using fusion strategy.



(b) Our proposed modality disentanglement strategy.

Fig. 1. Comparison of multi-contrast MRI reconstruction strategies. (a) Fusion-based approaches fuse the undersampled target image I_{tar}^{us} with the high-quality reference image I_{ref} , which may introduce irrelevant features. (b) Our proposed disentanglement-based method first complements the under-sampled target K-space using the reference modality, generating a structure-preserved but modality-mixed image I_{mix}^{fs} . A modality disentanglement network then removes reference-specific features to yield a clean target reconstruction I_{tar} .

among multiple coils to reconstruct the full-resolution image. However, despite their theoretical foundations, traditional algorithms often suffer from compromised image fidelity and long reconstruction times, hindering their practical deployment in real-world clinical environments.

Modern deep learning approaches [4] have improved reconstruction fidelity and computational efficiency, making them increasingly viable for clinical adoption. Some deep learning frameworks [5]–[9] treat MRI reconstruction as an image-domain task, neglecting the complex-valued nature of raw k-space data and its vital phase information, which is indispensable for functional and quantitative MRI applications. Therefore, dual-domain methods [10]–[13] attempt to bridge this gap by jointly optimizing image and frequency-domain representations, yet challenges persist in utilizing different domain information. Overcoming these limitations is essential for translating accelerated MRI into routine practice, particularly for time-sensitive diagnoses (e.g., stroke or dynamic contrast-enhanced studies) and resource-constrained settings.

Another promising direction is multi-contrast MRI reconstruction, which leverages complementary information across different contrast modalities. Since some modalities (e.g., T1)

Corresponding author: Juncheng Li (jcli@cs.ecnu.edu.cn)

Weiye Lyu, Xinming Fang, Jun Wang, and Jun Shi are with the School of Communication and Information Engineering, Shanghai University, Shanghai 200444, China.

Guixu Zhang and Juncheng Li are with the School of Computer Science and Technology, East China Normal University, Shanghai 200062, China.

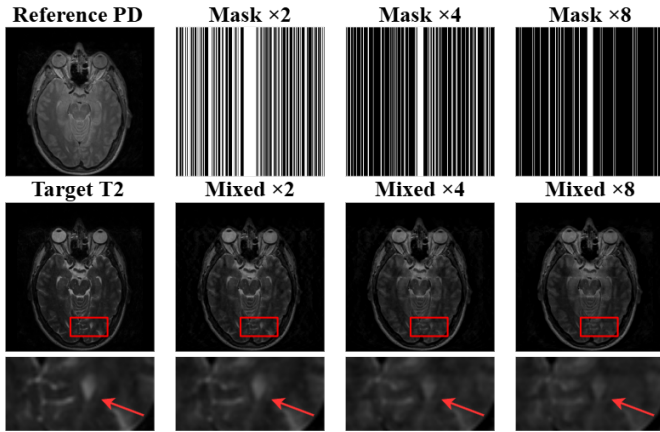


Fig. 2. Visualization of modality-mixed images generated under different accelerations. As the undersampling factor increases, more information is borrowed from the reference modality, resulting in a hybrid reconstruction that exhibits enhanced PD-like contrast (e.g., higher gray matter intensity and reduced T2-specific fluid signal).

can be acquired faster, they may serve as references to assist the reconstruction of slower modalities (e.g., T2). As shown in Fig. 1 (a), multi-contrast reconstruction approaches typically employ a dual-branch architecture that processes undersampled target images alongside fully-sampled reference images, subsequently fusing their complementary information. While existing methods primarily concentrate on optimizing fusion strategies [14], this paradigm inherently introduces extraneous information that may compromise reconstruction fidelity. In contrast, our approach fundamentally rethinks this framework by directly utilizing the reference modality to complete the undersampled target K-space data, thereby transitioning from feature fusion to feature disentanglement as shown in Fig. 1 (b). This paradigm shift guarantees structurally preserved inputs with suppressed artifacts for subsequent reconstruction stages.

Specifically, we propose **MambaMDN**, a new dual-domain framework for multi-contrast MRI reconstruction that integrates the K-space complementation strategy with an image-domain modality disentanglement module. In the K-space domain, we explicitly leverage the fully sampled reference modality to fill the missing K-space lines in the undersampled target measurement. This step is conceptually related to the Keyhole method [15] used in dynamic MRI, where central K-space from a reference frame of the same modality (e.g., before or after contrast agent injection) is substituted to accelerate acquisition. However, unlike Keyhole, which assumes the reference and target share the same contrast and only differ in temporal dynamics, our approach uses cross-contrast reference data, which can preserve anatomical structure but inevitably introduces modality-specific features into the target domain, as shown in Fig. 2. To handle these, we introduce a cross-modal feature disentanglement module inspired by the Mamba model [16] in the image domain. Specifically, we project the modality-mixed images and reference images into a high-dimensional feature space and apply a gating mechanism to extract the modality-specific features. Then, we subtract

the reference-specific features from the mixed representation to obtain features aligned with the target modality, thereby suppressing cross-modal interference while preserving features essential for accurate reconstruction. In addition, we design a progressive improvement mechanism to gradually improve disentanglement performance. In summary, the contributions of this paper can be summarized as follows:

- 1) We propose a novel method that utilizes fully-sampled reference K-space data to complete undersampled target acquisitions, generating structurally aligned yet modality-mixed inputs while preserving essential anatomical information.
- 2) We develop an innovative network architecture leveraging Mamba models to effectively separate and remove reference-specific features from mixed representations, addressing the critical challenge of information contamination in multi-contrast fusion.
- 3) We introduce a progressive refinement strategy to cyclically improve the reconstruction quality through repeated feature disentanglement, achieving superior artifact suppression compared to traditional reconstruction methods.

II. RELATED WORK

A. Multi-Contrast MRI Reconstruction

Single-contrast methods [17]–[20] are limited by the amount of available information within a single contrast, which may lead to ambiguity in anatomical structures and poor preservation of fine details. To address these limitations, multi-contrast MRI reconstruction has emerged as a promising strategy by exploiting the complementary information across different contrasts (e.g., T1, T2, PD). Early works [21], [22] have demonstrated improved performance over individual reconstruction by modeling structural consistency across modalities, typically through group sparsity, joint TV regularization, or shared gradient priors.

Some deep learning methods [23]–[25] use concatenated contrasts as input and fuse the features through neural networks. Dual-path approaches [18], [26], [27] employ separate branches for the reference and target modalities, allowing the fusion module to combine multi-scale features extracted from each modality. In addition, model-driven learning methods [28]–[32] embed mathematical priors into the network design by unrolling iterative optimization steps guided by predefined MRI objectives, thus emulating traditional reconstruction pipelines within a learnable framework.

However, these methods place their focus on fusing complementary information, without noticing that introducing reference modality will introduce irrelevant features. In contrast, converting multi-modal reconstruction into a disentanglement problem may achieve better results.

B. Dual-Domain MRI Reconstruction

MRI essentially operates in the frequency domain, where aliasing artifacts are introduced by undersampling of K-space. While image-domain methods treat reconstruction as a visual task, they often discard valuable frequency-domain priors.

On the other hand, methods that solely operate in K-space [33], [34] often rely on specific sampling patterns, limiting their adaptability and generalization across diverse acquisition settings.

To address the limitations of single-domain strategies, an increasing number of studies have investigated dual-domain frameworks that jointly leverage spatial and frequency information [10], [13], [35], [36]. KIKI-net [10] introduces a hybrid architecture where data consistency (DC) layers are inserted between K-space and image-domain networks, enabling cross-domain feature refinement. Wang et al. [13] pointed out that sharing the same architecture across domains may hinder domain-specific learning, and proposed customized subnetworks to better extract features from each domain. Ran et al. [35] observed that many dual-domain methods process K-space and image-domain data sequentially without explicit interaction. To overcome this, they proposed parallel branches that handle both domains simultaneously with cross-domain communication. Jiang et al. [36] introduced a contextual memory mechanism that facilitates iterative information exchange, allowing the model to utilize reconstruction knowledge from previous stages to enhance optimization.

However, due to the distinct statistical properties of K-space data, deep learning models designed for visual tasks often fail to generalize well in the frequency domain. Therefore, using the reference modality to complete the target K-space and using deep networks to decouple and reconstruct features in the image domain is a potential solution.

C. Mamba-based MRI Reconstruction

The Mamba model [16], based on a selective state-space mechanism, has recently shown strong potential in both language and vision tasks due to its efficient sequence modeling and linear time complexity. V-Mamba [37] extended this idea to vision by introducing a two-dimensional selective scan (SS2D), enabling effective spatial context modeling. Compared to Transformers and CNNs, Mamba offers improved long-range dependency modeling with significantly lower computational complexity and memory usage, making it particularly suitable for high-resolution medical imaging tasks such as MRI reconstruction.

Based on these advances, recent works have begun to explore Mamba for MRI reconstruction [38]–[42]. Korkmaz et al. [40] proposed a lightweight framework that alternates between Mamba and data consistency blocks. Ji et al. [41] proposed a Deform-Mamba encoder featuring two distinct branches: a modulated deformable block and a vision-oriented Mamba module for feature extraction. Meng et al. [42] introduced a circular scanning approach to better model and retain the structure of the K-space data. Inspired by these works, we aim to integrate the SS2D module into our modality disentanglement module, enabling long-range feature modeling and effective suppression of reference interference in the image domain.

III. METHOD

A. Preliminaries

1) *MRI Reconstruction*: MRI reconstruction aims to recover an image $\mathbf{x} \in \mathbb{C}^n$ from its frequency-domain measurements. The fully-sampled K-space $\mathbf{y}^{fs} \in \mathbb{C}^n$ is related to the ground-truth image through the following forward model [14]:

$$\mathbf{y}^f = \mathcal{F}\mathbf{x} + \eta, \quad (1)$$

where $n = n_1 \times n_2$ indicates the resolution in K-space, η represents complex Gaussian noise with distribution $\mathcal{CN}(0, \Sigma)$, \mathcal{F} denotes the two-dimensional Fourier transform.

In the multi-coil setting, $\mathbf{y} = (y_1, y_2, \dots, y_{n_c})$ denote the full set of undersampled measurements across n_c coils. The forward model can be expressed as:

$$\mathbf{y} = \mathcal{M} \odot \mathcal{F}\mathbf{S}\mathbf{x} + \eta = \mathbf{A}\mathbf{x} + \eta, \quad (2)$$

where $\mathbf{A} = \mathcal{M} \odot \mathcal{F}\mathbf{S}$ is the linear forward operator, $\mathbf{S} = (\mathbf{S}_1, \mathbf{S}_2, \dots, \mathbf{S}_{n_c})$ denotes the coil sensitivity maps, and $\mathcal{M} \odot$ represents an element-wise undersampling mask.

Deep learning-based reconstruction aims to estimate a high-quality image $\hat{\mathbf{x}}$ by learning a mapping from undersampled K-space data \mathbf{y} , typically using the following formulation:

$$\hat{\mathbf{x}} = f_{NET}(\text{IFFT}(\mathbf{y}); \theta), \quad (3)$$

where θ denotes parameters of the network and $\text{IFFT}(\mathbf{y})$ represents the zero-filled initial reconstruction obtained by applying the inverse Fourier transform to the undersampled K-space data.

In this work, we focus on the single-coil simulation setting, where the sensitivity maps are not explicitly estimated or used. However, it can be extended to multi-coil reconstruction by incorporating a sensitivity map estimation module or adapting the input pipeline to handle coil-wise data.

2) *The Mamba Model and SS2D*: Structured State Space Models (SSMs) offer a systematic approach to capturing long-range dependencies through linear dynamics within a latent space. The continuous-time SSM is given by the following set of ordinary differential equations:

$$\begin{cases} \frac{dh(t)}{dt} = Ah(t) + Bx(t), \\ y(t) = Ch(t) + Dx(t), \end{cases} \quad (4)$$

where $x(t)$ is the input sequence, $h(t)$ is the latent state, $y(t)$ is the output. $A \in \mathbb{R}^{N \times N}$, $B \in \mathbb{R}^{N \times 1}$, $C \in \mathbb{R}^{1 \times N}$, and $D \in \mathbb{R}$ are learnable parameters. Meanwhile, the term $Dx(t)$ serves as a skip connection, enhancing gradient flow and representation capacity.

To incorporate the system into deep networks, zero-order hold (ZOH) discretization is applied with step size Δ . The resulting recurrence formulation is given by:

$$\begin{cases} h_k = Ah_{k-1} + Bx_k, \\ y_k = Ch_k + Dx_k, \end{cases} \quad (5)$$

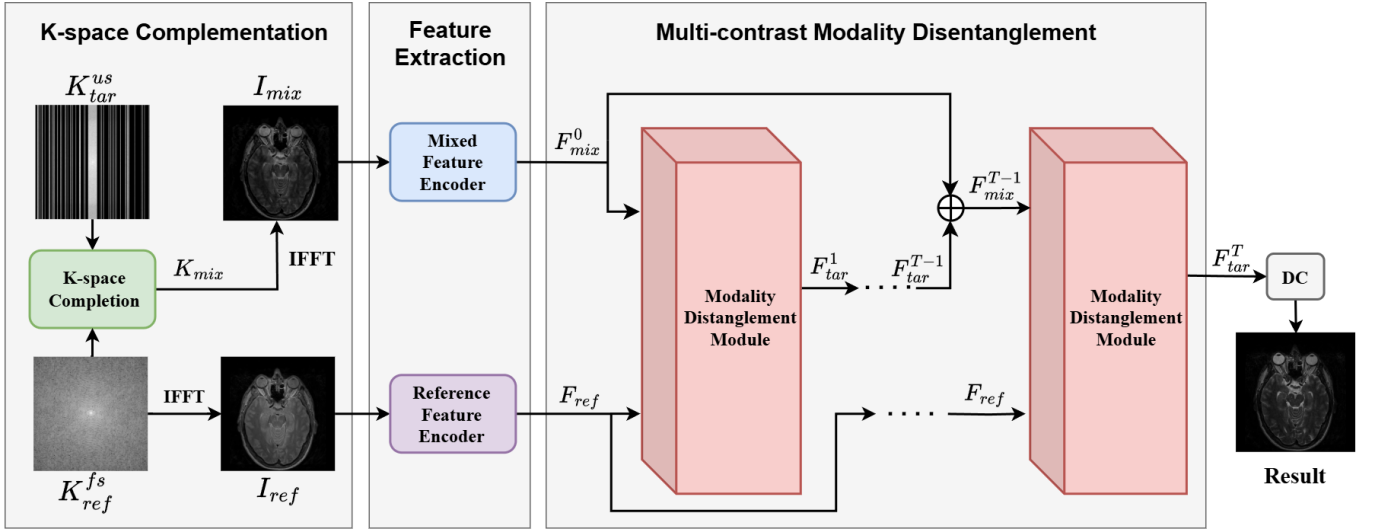


Fig. 3. Overview of the proposed MambaMDN framework. The undersampled target K-space data K_{tar}^{us} is complemented by the fully sampled reference data K_{ref}^{fs} to generate a contrast-mixed image I_{mix} . Furthermore, we use two encoders to extract high-level features F_{mix} and F_{ref} , which are progressively disentangled by Mamba-based modules to reconstruct the target image. Finally, a DC layer is employed to ensure data consistency to get the final result.

where $A = \exp(\Delta A)$ and $B = (\Delta A)^{-1}(\exp(\Delta A) - I) \cdot \Delta B$ are the discretized parameters. This formulation can be further expressed in a convolutional form:

$$\begin{cases} y = x * K, \\ K = [CB, CAB, \dots, CA^{L-1}B], \end{cases} \quad (6)$$

where L is the sequence length and $K \in \mathbb{R}^L$ is the SSM convolution kernel used to encode the temporal dynamics of the system.

Base on this foundation, the Mamba model [16] introduces the Selective State Space (S6) mechanism, which dynamically generates the parameters B , C , and Δ in a data-dependent manner. This selective parameterization enables the model to modulate information flow based on the input, enabling efficient and scalable modeling of long-range dependencies with linear time complexity.

To extend SSMs to visual tasks, V-Mamba [37] proposes the Selective Scan 2D (SS2D) mechanism, which adapts the selective scanning process to two-dimensional spatial inputs. Unlike traditional one-dimensional scanning that processes tokens sequentially, SS2D performs directional scanning along four spatial directions, thereby capturing contextual information from multiple geometric perspectives. This design bridges the gap between the sequential nature of state space models and the grid-like structure of visual data.

B. MambaMDN

The proposed MambaMDN architecture, illustrated in Fig. 3, comprises three key stages: (1) K-space complementation, (2) feature extraction, and (3) multi-contrast modality disentanglement. The framework accepts two inputs: undersampled target K-space data and fully-sampled reference K-space data. Specifically, the K-space Complementation Module (KCM) first processes these inputs to generate contrast-mixed K-space data, which is subsequently transformed to the image

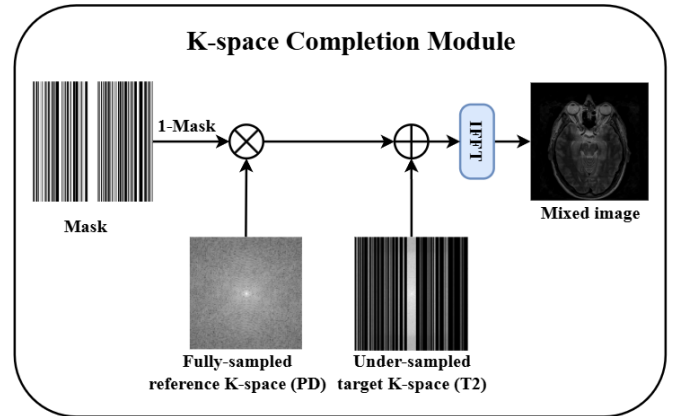


Fig. 4. The proposed KCM module. The fully-sampled reference (PD) image is transformed to the K-space domain and used to fill the missing regions of the undersampled target (T2) K-space, yielding an artifact-free but modality-mixed image for the reconstruction network.

domain via inverse fast Fourier transform (IFFT). During feature extraction, dedicated modality-specific encoders extract discriminative features from both the mixed representation and reference modality. Finally, the modality disentanglement network, which is based on the Mamba model, leverages the reference features to identify and suppress reference-specific components in the mixed representation, enabling accurate reconstruction of the target modality.

1) *K-space Complementation Module*: The zero-filled target image is commonly used as the input in many existing reconstruction methods. However, the aliasing artifacts and structural blurring in the image domain severely degrade fine anatomical detail recovery and increase the learning difficulty of the reconstruction network.

To address this limitation, our K-space Complementation Module (KCM) is introduced to generate a modality-mixed image by leveraging the available different contrast informa-

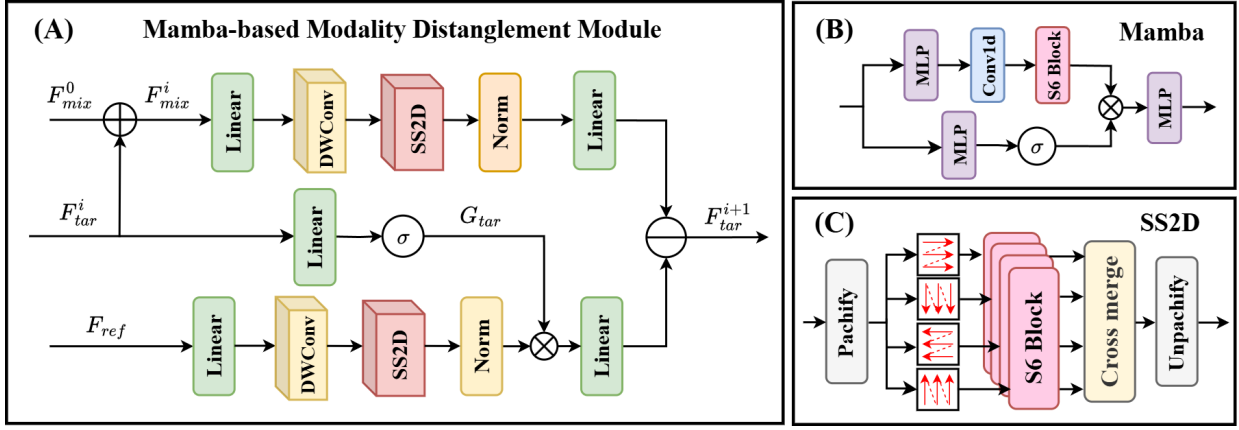


Fig. 5. Illustration of the proposed Mamba-based Modality Disentanglement (MMD) module. (A) The overall structure of MMD disentangles modality-specific features from the mixed representation using reference modulation. (B) The original Mamba block. Inspired by it, we designed our MMD module. (C) The SS2D block proposed by Vmamba [37] enables the MMD to effectively model spatially long-range features.

tion. As shown in Fig. 2, the output of the KCM preserves more structural details and reduces aliasing compared to the zero-filled input, providing a stronger prior for the downstream reconstruction network. In this way, we shift the learning focus from traditional aliasing removal to modality disentanglement. The inner operation is shown in Fig. 4, which can be summarized by:

$$\begin{cases} K_{mix} = K_{tar}^{us} + (1 - M) \odot K_{ref}^{fs}, \\ I_{mix} = \text{IFFT}(K_{mix}), \end{cases} \quad (7)$$

where M is the binary sampling mask, \odot is the element-wise multiplication, K_{tar}^{us} is the input undersampled target data, K_{ref}^{fs} is the fully sampled reference data, and I_{mix} is the feature-mixed image transformed from mixed K-space data K_{mix} via IFFT.

By explicitly complementing the missing K-space regions with structurally similar information from a fully-sampled reference contrast, KCM reduces aliasing and preserves fine anatomical details that are otherwise difficult to recover. This initialization not only guides the network away from overfitting to noise under high acceleration factors (e.g., $\times 8$), but also improves the stability and convergence of training.

2) *Feature Extraction Module*: To enable more expressive representation learning, we repeat the input images from a single channel to c channels before feeding them into the feature encoders. Then we employ two encoders: a Mixed Feature Encoder (MFE) to process the feature-mixed image from the KCM module, and a Reference Feature Extractor (RFE) to extract features from the fully sampled reference modality. Although both networks share a U-Net backbone, they serve different purposes:

- (1) The MFE takes the mixed image I_{mix} as input and extracts mixed representations F_{mix}^0 . These features serve as the initial input to the subsequent modality disentanglement network.

$$F_{mix}^0 = \text{MFE}(I_{mix}). \quad (8)$$

- (2) The RFE processes the clear reference images I_{ref} to generate a high-level representation F_{ref} , which is for-

warded to each modality disentanglement block to extract reference-specific features, thereby facilitating more accurate reconstruction of the target modality.

$$F_{ref} = \text{RFE}(I_{ref}). \quad (9)$$

3) *Mamba-based Modality Disentanglement Module*: On the basis of introducing multi-contrast information to enhance undersampled K-space data, we need to distinguish between target modal features and modal-mixed features. To achieve this, we propose a Mamba-based Modality Disentanglement (MMD) module, as illustrated in Fig. 5 (A). Inspired by the Mamba model [16] shown in Fig. 5 (B), we extend its original architecture to accept two inputs, and connect the gating branch (with activation σ) to the reference branch for adaptive modulation. Moreover, to make the module suitable for 2D inputs, we replace the 1D convolution and S6 block with a depthwise convolution and the SS2D block [37], as illustrated in Fig. 5 (C). These adaptations enable the MMD module to progressively filter out reference-specific features, ensuring accurate reconstruction of the target modality.

Specifically, this module takes the intermediate feature F_{tar}^i and the extracted reference feature F_{ref} as input, and outputs a refined, target-specific representation F_{tar}^{i+1} . F_{tar}^i is obtained by a residual connection between the previous target feature F_{tar}^i and the original mixed feature F_{mix}^0 :

$$F_{mix}^i = F_{mix}^0 + F_{tar}^i, 0 < i \leq T \quad (10)$$

where F_{mix}^i and F_{tar}^i are initialized as F_{mix}^0 , which is obtained by the MFE.

Both F_{mix}^i and F_{ref} are first passed through the lightweight linear projection. In addition, a depthwise convolution followed by an SS2D block is applied to enhance spatial modeling and long-range contextual interactions. These components ensure structured feature extraction with low computational cost. Meanwhile, a gating mechanism is introduced to adaptively regulate the disentanglement. The modulation gating parameters G_{tar}^i is generated via:

$$G_{tar}^i = \sigma(\text{Linear}(F_{tar}^i)), \quad (11)$$

where $\sigma(\cdot)$ is an activation function. G_{tar}^i can be used to modulate the reference feature, and the gated information is subtracted from the mixed feature path:

$$F_{tar}^{i+1} = \tilde{F}_{mix}^i - \text{Linear}(G_{tar} \odot \tilde{F}_{ref}), \quad (12)$$

where \tilde{F}_{mix}^i and \tilde{F}_{ref} denote the respective features after projection, depthwise convolution, SS2D, and normalization. The symbol \odot denotes element-wise multiplication.

This design enables modality-aware disentanglement by adaptively suppressing irrelevant features from the reference modality while preserving target-specific information. Unlike fusion strategies that risk injecting misleading information from the reference modality, particularly when modality-specific features (e.g., low fluid sensitivity in PD or high contrast of white matter in T1) are inconsistent with the target, our module filters out reference-specific components, ensuring that the final representation is aligned with the target modality.

Finally, we apply a data consistency (DC) layer after the final MMD block. The DC layer can ensure that the reconstruction conforms to the observed K-space data, learns stably, and preserves fine anatomical details.

4) *Progressive Refinement Mechanism*: To improve disentanglement performance, we implement a progressive refinement strategy through multi-stage application of our MMD module. At each iteration i ($1 \leq i \leq T$), the module progressively suppresses reference-specific components from the mixed features using intermediate outputs from the preceding stage. This iterative design enables gradual correction of cross-modal interference, progressively enhancing feature purity and target-modality consistency. Consequently, our MMD module effectively mitigates modality confusion from K-space complementation while improving reconstruction fidelity.

5) *Loss Function*: Our network is trained in an end-to-end manner, employing the standard pixel-wise L1-loss as the loss function. Specifically, the loss function is applied between the reconstructed target image \hat{I}_{tar} and the fully sampled ground truth data K_{tar}^{fs} :

$$LL1 = |\hat{I}_{tar} - \text{IFFT}(K_{tar}^{fs})|_1. \quad (13)$$

This simple yet effective loss encourages accurate pixel-level recovery and stable convergence.

IV. EXPERIMENTS

A. Data Preparation

1) *Dataset*: In this work, we use three public multi-contrast datasets to evaluate the effectiveness of the proposed method, including the IXI dataset, the BraTS dataset, and the M4raw dataset.

IXI Dataset: In this dataset, we employ PD modality as the reference and T2 modality as the target. Each modality consists of 576 MRI volumes, which are split into a ratio of 7:1:2 for train, valid, and test sets. The middle 100 slices in each volume are selected for our experiments. Each slice of this dataset has a resolution of 256×256 .

BraTS: BraTS [43] contains a collection of 285 multi-contrast MR volumes. It was split into a ratio of 7:1:2 for training, validating, and testing. T1 is regarded as the reference

modality to direct the reconstruction of the target T2 modality. Similar to the IXI dataset, we only utilize the middle 100 slices for our experiments, and each slice has a resolution of 240×240 .

M4raw: M4raw [44] is a multi-contrast and multi-channel MRI dataset containing T1, T2, and FLAIR contrast. In our experiments, we filter out 150 paired T1 and T2 brain volumes for our model evaluation, and each volume has 18 slices with 256×256 resolution. These slices are split into a ratio of 7:1:2 for training, validating, and testing. T1 modality is directed toward the restoration of T2 modality.

2) *Mask*: In this work, we adopt a variable-density random sampling mask along the phase-encoding direction to simulate undersampled K-space data. Specifically, we use acceleration factors of $\times 4$ and $\times 8$ to evaluate the model under both moderate and high undersampling scenarios. Each mask retains a fixed low-frequency region in the center to preserve structural information, while the remaining frequencies are randomly sampled with a probability determined by the desired acceleration rate. A fixed random seed is used to ensure reproducibility.

B. Evaluation Metrics and Experimental Setup

In this work, we quantitatively evaluated our model using three standard metrics: peak signal-to-noise ratio (PSNR), structural similarity index (SSIM), and root mean square error (RMSE). These metrics were computed on image-domain reconstructions obtained through inverse Fourier transform of the processed K-space data. Following convention, superior reconstruction quality is indicated by higher PSNR/SSIM values and lower RMSE values.

Our experimental implementation utilizes the PyTorch framework running on NVIDIA GeForce RTX 3090 GPUs. In the training phase, we employed the Adam optimizer with a learning rate of 1×10^{-4} and batch size of 6 for 50 training epochs. For the final model, the channel number c is expanded to 32 after the KCM module, and the number of MMD modules is set to 6.

C. Quantitative Comparison

We conducted a comparative evaluation of the proposed MambaMDN against several existing MRI reconstruction methods to demonstrate its effectiveness, including single-contrast baselines such as U-Net [45], Restormer [46], and MambaRecon [40], as well as multi-contrast methods like MC-VANet [28], PanMamba [47], and MambaMMR [48]. TABLE I reports the quantitative results of these models on IXI, BraTS, and M4raw datasets under $\times 4$ and $\times 8$ acceleration settings.

As shown in TABLE I, our MambaMDN achieves the best performance across all metrics and datasets. For instance, on the IXI dataset with $\times 4$ acceleration, MambaMDN surpasses MC-VANet and MambaRecon by 1.15 dB and 2.26 dB in PSNR, respectively. On the more challenging $\times 8$ setting, MambaMDN still maintains a clear margin, outperforming MC-VANet by 1.10 dB. Similarly, on the BraTS and M4raw dataset, our method achieves the highest PSNR and SSIM under both acceleration factors. It is worth noting that although

TABLE I
QUANTITATIVE COMPARISON ON IXI, BRATS, AND M4RAW DATASETS UNDER $\times 4$ AND $\times 8$ ACCELERATION RATES. BEST RESULTS AND SECOND-BEST RESULTS ARE HIGHLIGHTED AND UNDERLINED, RESPECTIVELY.

Dataset	Methods	$\times 4$ Acceleration			$\times 8$ Acceleration		
		PSNR (dB) \uparrow	SSIM \uparrow	RMSE \downarrow	PSNR (dB) \uparrow	SSIM \uparrow	RMSE \downarrow
IXI	Zero-Filled (ZF)	24.60	0.5420	15.94	23.39	0.4995	18.31
	U-Net [45] (MICCAI 2015)	31.95	0.9032	6.933	30.66	0.8875	7.980
	Restormer [46] (CVPR 2022)	38.10	0.9693	3.417	36.46	0.9629	4.046
	MC-VANet [28] (ICCV 2023)	<u>40.77</u>	<u>0.9778</u>	<u>2.510</u>	<u>38.20</u>	<u>0.9681</u>	<u>3.354</u>
	PanMamba [47] (IF 2025)	39.01	0.9703	3.048	<u>37.56</u>	<u>0.9650</u>	3.602
	MambaRecon [40] (WACV 2025)	39.66	0.9708	2.838	36.76	0.9588	3.918
	MambaMMR [48] (MedIA 2025)	38.41	0.9636	3.259	37.10	0.9632	3.747
	MambaMDN (ours)	41.92	0.9806	2.211	39.30	0.9724	2.981
BraTS	Zero-Filled (ZF)	24.65	0.5642	15.17	24.37	0.5630	15.66
	U-Net [45] (MICCAI 2015)	30.90	0.9140	7.404	29.27	0.8905	8.944
	Restormer [46] (CVPR 2022)	34.21	0.9506	5.071	33.24	0.9429	5.667
	MC-VANet [28] (ICCV 2023)	37.75	0.9699	3.390	<u>35.55</u>	<u>0.9573</u>	4.364
	PanMamba [47] (IF 2025)	36.29	0.9659	4.005	34.84	0.9567	4.732
	MambaRecon [40] (WACV 2025)	36.84	0.9594	3.745	34.87	0.9484	4.695
	MambaMMR [48] (MedIA 2025)	<u>37.92</u>	<u>0.9709</u>	<u>3.292</u>	35.54	0.9568	4.330
	MambaMDN (ours)	38.18	0.9727	3.228	35.84	0.9606	4.214
M4raw	Zero-Filled (ZF)	24.36	0.6014	15.52	23.14	0.5141	17.86
	U-Net [45] (MICCAI 2015)	28.96	0.7572	9.150	26.46	0.6639	12.20
	Restormer [46] (CVPR 2022)	30.84	0.7692	7.367	29.08	0.7219	9.021
	MC-VANet [28] (ICCV 2023)	<u>31.82</u>	<u>0.8161</u>	<u>6.576</u>	28.70	0.7107	9.424
	PanMamba [47] (IF 2025)	31.58	0.8146	6.759	<u>29.13</u>	<u>0.7276</u>	<u>8.973</u>
	MambaRecon [40] (WACV 2025)	29.42	0.7391	8.673	27.11	0.6380	11.30
	MambaMMR [48] (MedIA 2025)	29.52	0.7507	8.576	28.19	0.7035	9.994
	MambaMDN (ours)	32.01	0.8205	6.435	29.75	0.7310	8.347

MambaMMR [48] and MC-VANet [28] are also multi-contrast reconstruction methods, their performance lags behind our MambaMDN. This highlights the effectiveness of our modality disentanglement strategy, which allows MambaMDN to better exploit complementary information from the reference modality while preserving target-specific features.

D. Qualitative Results

Figs. 6, 7, and 8 present qualitative comparisons of these models on IXI, BraTS, and M4raw datasets, respectively. Group (A) corresponds to 1D random undersampling with $\times 4$ acceleration rate, while Group (B) corresponds to $\times 8$ setting. In addition, the first row of each group shows the reconstruction result, while the second row indicates the error map. Obviously, our MambaMDN achieves superior preservation of structural details and significantly reduces reconstruction errors compared to other methods. The proposed framework consistently maintains high-fidelity texture representation and precise anatomical boundary delineation across varying undersampling rates, exhibiting remarkable robustness and versatile adaptation to different acquisition scenarios.

These improvements are not only beneficial in a technical sense but also particularly meaningful in clinical contexts, where accurate visualization of anatomical structures is essential for reliable interpretation. This is especially evident in the IXI dataset, which comprises healthy brain scans with clear and consistent structural features. Our method performs

notably well in this setting, highlighting its strong capacity to preserve fine-grained anatomical details, which is important for clinical scenarios that rely on high-resolution imaging of normal tissue morphology.

E. Model Complexity

As shown in TABLE II, we compared the FLOPs, memory consumption, and reconstruction performance of multiple models based on Mamba and Transformer on the IXI dataset (batch size=4). Notably, Mamba-based methods (PanMamba, MambaRecon, MambaMMR, and our MambaMDN) exhibit superior computational efficiency. Our MambaMDN achieves the best reconstruction result with moderate resource requirements, demonstrating its effectiveness in joint spatial-modality feature modeling. Compared to Transformer-based Restormer and model-driven MC-VANet, MambaMDN reduces computational costs by 30.7% and 74.1% respectively while delivering superior reconstruction fidelity. Therefore, we can draw a conclusion that our MambaMDN achieves the best balance between model complexity and performance.

V. ABLATION STUDY

A. Effectiveness of Modality Disentanglement Strategy

To evaluate the effectiveness of our proposed modality disentanglement strategy, we conduct ablation studies by comparing different disentanglement designs, as illustrated in Fig. 9.

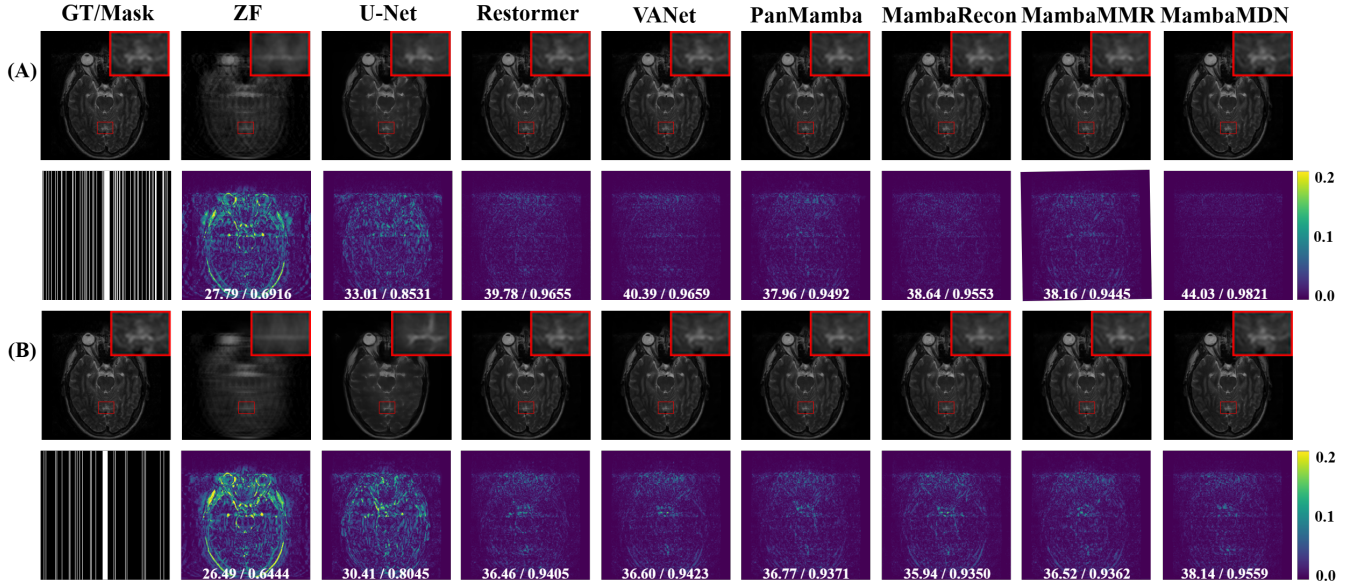


Fig. 6. Visual comparison of different methods on the IXI dataset. The first row of each group shows the reconstruction result, while the second row indicates the error map. Group (A) uses a 1D random undersampling mask with $\times 4$ acceleration rate, while Group (B) uses a $\times 8$ rate mask.

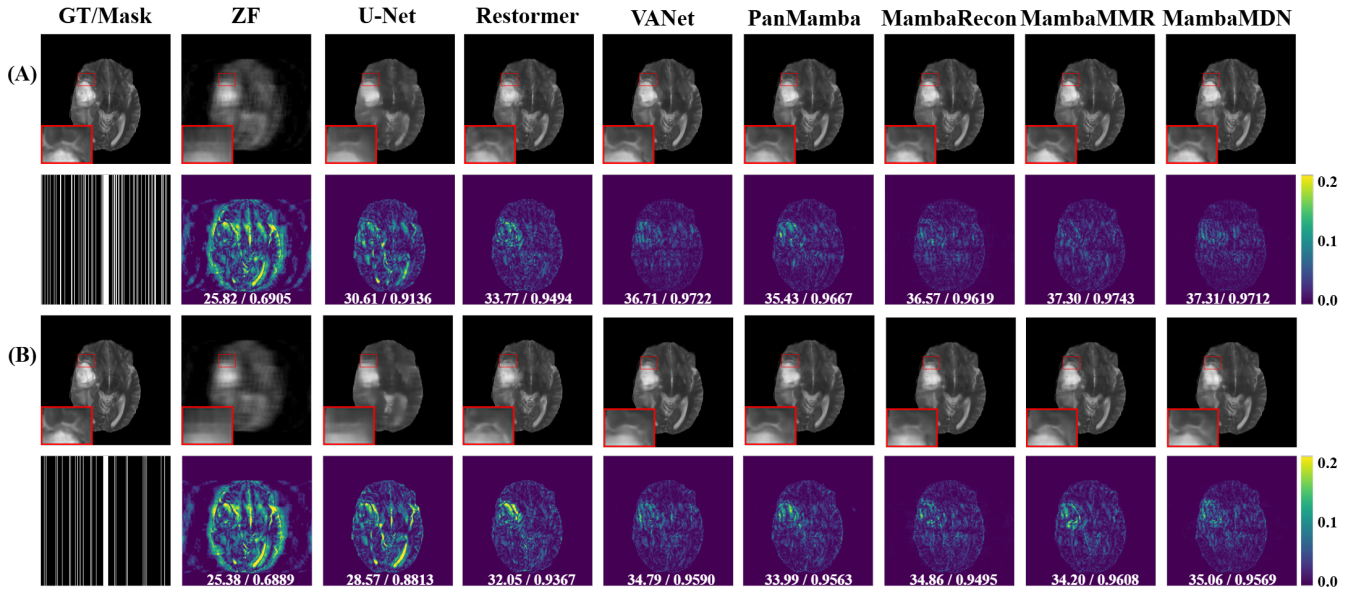


Fig. 7. Visual comparison of different methods on the BraTS dataset. The first row of each group shows the reconstruction result, while the second row indicates the error map. Group (A) uses a 1D random undersampling mask with $\times 4$ acceleration rate, while Group (B) uses a $\times 8$ rate mask.

The quantitative results on the IXI dataset are summarized in TABLE III, while Fig. 10 presents qualitative comparisons of the reconstructed images.

$F_{mix} - F_{ref}$ (ours): Our full method separates the target-relevant features by removing reference-specific information from the mixed representation, using fully sampled reference data. This produces the best results as it can accurately suppress irrelevant structures and better preserve target-specific content.

$F_{tar}^{us} - F_{ref}$: In this setting, we replace the KCM-generated input with the undersampled target modality directly. This lead to a 0.44 drop in PSNR and a 0.017 decrease in SSIM. Since

the gating mechanism is able to preserve target features and suppress reference interference, the disentanglement module still works even when starting from an aliased target. However, the presence of noise and aliasing in the undersampled target can hinder the gating’s ability to distinguish between useful structures and artifacts, thus reducing the overall quality of the disentanglement.

$F_{mix} - F_{tar}^{us}$: This design subtracts the undersampled target features from the mixed representation. Theoretically, this operation will get reference-specific features, which is contradictory to our goal of reconstructing the target modality. As a result, the reconstruction performance drops the most,

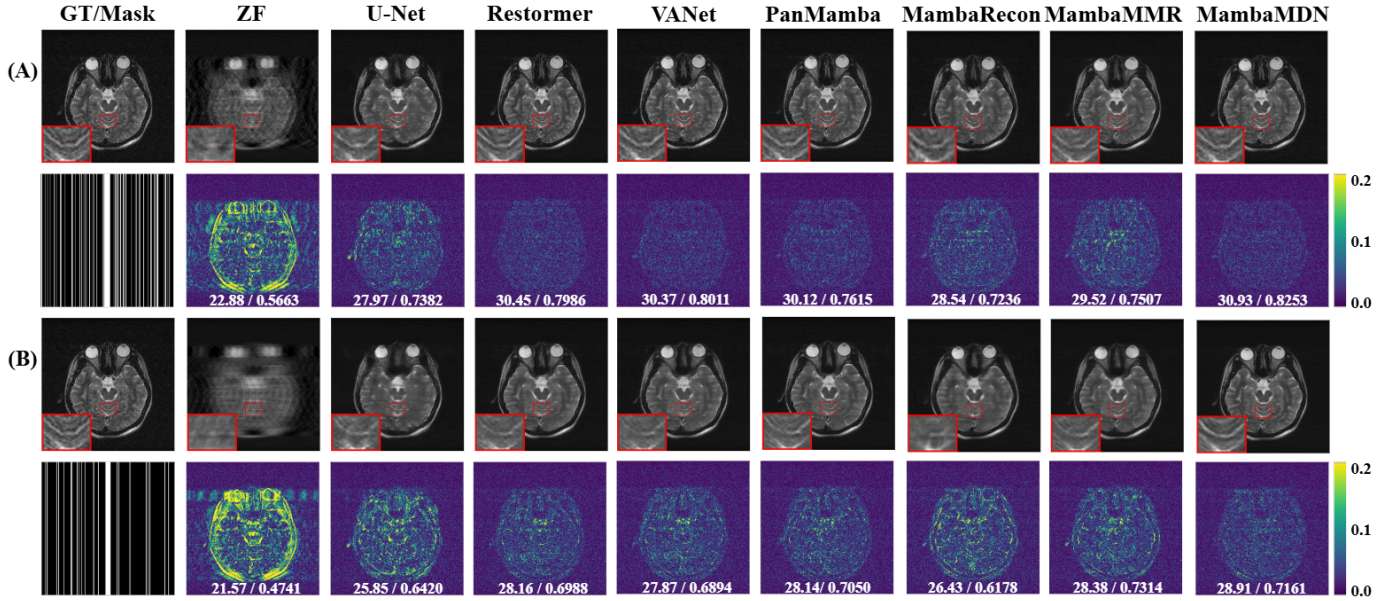


Fig. 8. Visual comparison of different methods on the M4raw dataset. The first row of each group shows the reconstruction result, while the second row indicates the error map. Group (A) uses a 1D random undersampling mask with $\times 4$ acceleration rate, while Group (B) uses a $\times 8$ rate mask.

TABLE II

QUANTITATIVE COMPARISON OF MODEL COMPLEXITY (FLOPS, MEMORY, AND RECONSTRUCTION QUALITY) ON THE IXI DATASET WITH BATCH SIZE = 4.

Methods	FLOPs	Memory	PSNR	SSIM
U-Net [45]	35.86G	1.42GB	31.95	0.9032
Restormer [46]	161.92G	26.42GB	38.10	0.9693
PanMamba [47]	76.17G	10.43GB	39.01	0.9703
MambaRecon [40]	30.29G	5.66GB	39.66	0.9708
MambaMMR [48]	99.41G	11.98GB	38.41	0.9636
MC-VANet [28]	432.62G	12.55GB	40.77	0.9778
MambaMDN (ours)	112.15G	7.86GB	41.92	0.9806

TABLE III

COMPARISON OF DIFFERENT MODALITY DISENTANGLEMENT STRATEGIES ON THE IXI DATASET. THE BEST RESULTS ARE HIGHLIGHTED.

Strategy	PSNR \uparrow	SSIM \uparrow	RMSE \downarrow
$F_{mix} - F_{ref}$ (ours)	41.92	0.9806	2.211
$F_{tar}^{us} - F_{ref}$	41.48	0.9789	2.327
$F_{mix} - F_{tar}^{us}$	41.13	0.9762	2.411
$F_{mix} - 0$	41.33	0.9649	2.355

with a decrease of 0.79 dB in PSNR and 0.044 in SSIM.

(D) $F_{mix} - 0$: In this case, we modified the MMD module into a single-contrast version, forcing the model to perform modality self-conversion without any reference-specific guidance. Thanks to the de-aliased and structurally clean input provided by the KCM module, the model maintained reasonable pixel-level accuracy, evidenced by only a modest PSNR drop of 0.59 dB. However, the lack of reference guidance introduced noticeable cross-modal interference, significantly compromising structural fidelity and leading to a substantial

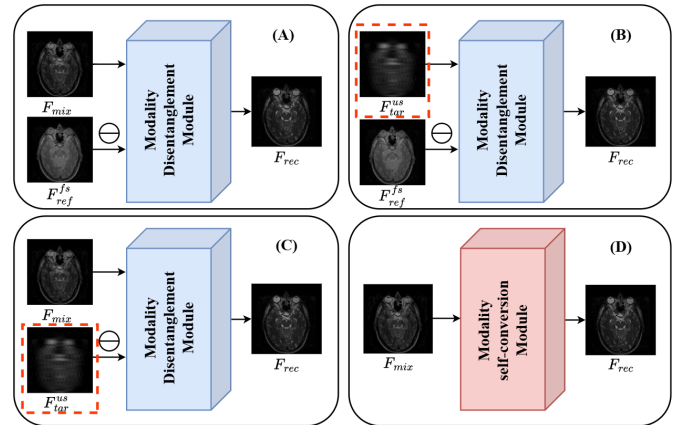


Fig. 9. Ablation study on disentanglement designs. (A) Our full model subtracts the reference features from the mixed modality. (B) Replacing the KCM-generated input with the undersampled target. (C) Replacing the subtraction input with the undersampled target leads to inaccurate disentanglement. (D) Removing the reference entirely forces the model to perform modality self-conversion.

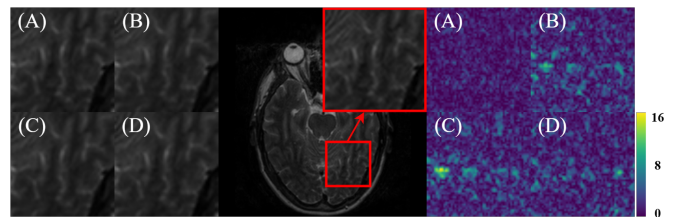


Fig. 10. Result of different modality disentanglement strategies. Our method achieved the best reconstruction result.

SSIM reduction of 0.0157.

TABLE IV
IMPACT OF MMD MODULE QUANTITY ON PERFORMANCE.

Number	PSNR \uparrow	SSIM \uparrow	RMSE \downarrow
4 blocks	41.51	0.9789	2.312
5 blocks	41.69	0.9797	2.266
6 blocks	41.92	0.9806	2.211
7 blocks	41.83	0.9802	2.231

TABLE V
RESULTS OF THE MODEL WITH AND WITHOUT ITERATIVE REFINEMENT STRATEGY ON THE IXI TEST SET.

Parallel or Iterative	PSNR \uparrow	SSIM \uparrow	RMSE \downarrow
6 iterative blocks (ours)	41.92	0.9806	2.211
6 parallel blocks	39.57	0.9713	2.860
single block	38.97	0.9683	3.063

B. Impact of MMD Module Quantity on Performance

To evaluate the impact of the MMD module count on reconstruction performance, we conducted ablation experiments on the IXI test set. As summarized in TABLE IV, increasing the number of MMD modules from 4 to 6 leads to progressive improvements in PSNR and SSIM alongside reduced RMSE, demonstrating enhanced image quality and more effective modality disentanglement. However, increasing to 7 modules causes performance degradation, likely due to feature over-subtraction. Based on these findings, we use 6 MMD modules in the final model to maximize reconstruction quality. Notably, the Mamba-based architecture’s lightweight design ensures this configuration maintains high computational efficiency without introducing substantial overhead.

C. Effectiveness of Iterative Refinement Strategy

To investigate the impact of the iterative refinement strategy on model performance, we designed an ablation experiment to compare the results with and without this strategy. Specifically, we conduct an ablation study where 6 MMD modules are employed without progressive refinement strategy. We stack 6 MMD modules in a parallel way, and they independently process the same input pair (F_{mix}^0, F_{ref}), then the outputs are averaged to get the final target result. As shown in Table 2, the performance of both ‘single block’ or ‘6 parallel blocks’ has decreased. In contrast, the model using our proposed iterative refinement strategy achieved the best results. This fully validates the effectiveness of the strategy.

D. Effectiveness of K-space Complementation Module

To evaluate the effectiveness of the proposed K-space Complementation Module (KCM), we removed the KCM from our MMD framework. In this setting, the model takes the undersampled target image I_{tar}^{us} and the fully sampled reference image I_{ref}^{fs} as input. We modify our disentanglement module to perform a fusion strategy, replacing the subtraction operation with feature addition. As shown in the last row of TABLE VI, removing the KCM led to a noticeable drop in

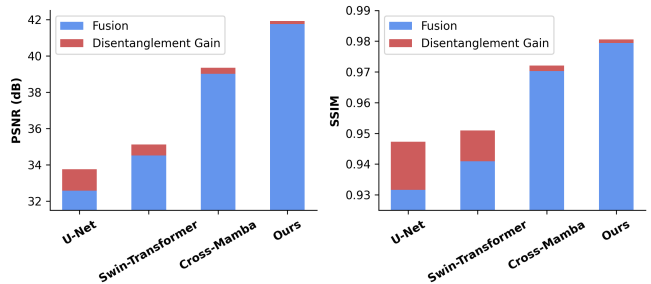


Fig. 11. Comparison of fusion and disentanglement strategies across different backbone architectures.

TABLE VI
COMPARISON BETWEEN DIFFERENT NETWORKS IN THE FEATURE INTERACTION STAGE.

Methods	Disentanglement			Fusion		
	PSNR \uparrow	SSIM \uparrow	RMSE \downarrow	PSNR \uparrow	SSIM \uparrow	RMSE \downarrow
U-Net [45]	33.75	0.9473	5.490	32.58	0.9316	6.260
SwinT [49]	35.12	0.9509	4.720	34.51	0.9409	5.083
Cross-M [47]	39.34	0.9721	2.939	39.01	0.9703	3.048
Ours	41.92	0.9806	2.211	41.75	0.9794	2.255

performance, 0.17 dB in PSNR and 0.0012 in SSIM, indicating that the input from K-space complementation provides more informative guidance than direct fusion.

Meanwhile, we evaluated the effectiveness of KCM across multiple backbone architectures, including U-Net [45], Swin Transformer [49], and Cross-Mamba [47]. For each backbone, we designed two variants: one that simply fuses (Fusion) and another that leverages the proposed KCM to produce a modality-mixed image, followed by a modality disentanglement strategy (Disentanglement). As shown in Fig. 11 and TABLE VI, among all architectures, the KCM-based disentanglement method consistently outperforms simple fusion. By directly combining the low-quality target K-space and the high-quality reference K-space using the undersampling mask, KCM reconstructs a cleaner and artifact-suppressed mixed image, which serves as a better input for downstream feature interaction. Notably, the improvements are more prominent in lighter architectures (e.g., U-Net and Swin Transformer), highlighting the generality and effectiveness of KCM as an enhancement module.

VI. DISCUSSION

In this study, we present MambaMDN, an innovative reconstruction paradigm that transforms multi-modal MRI from conventional feature fusion to anatomically-aware modality disentanglement. This approach addresses two problems: (1) our k-space complementation strategy helps preserve native tissue contrast during acquisition, reducing aliasing artifacts in the reconstructed images, and (2) the Mamba-based disentanglement module reduces interference from reference anatomy, which may improve feature specificity and aid lesion visualization.

Regarding potential clinical use, MambaMDN demonstrates the ability to reconstruct target contrasts (e.g., T2-weighted) from substantially undersampled acquisitions when aided by reference scans (e.g., T1-weighted). Meanwhile, the computational efficiency of the method makes it promising for clinical deployment. Compared to existing solutions requiring GPU clusters, MambaMDN offers a favorable balance between reconstruction performance and resource consumption, which is especially valuable in time-sensitive or resource-limited settings such as rural clinics, emergency treatment, and low-field MRI systems.

Although our MambaMDN demonstrates strong reconstruction performance, several limitations remain. First, residual cross-modal contamination still persists in the critical anatomical region, and conventional pixel-wise metrics inadequately capture diagnostic fidelity for pathological tissues, suggesting the need for lesion-aware optimization criteria that prioritize clinically relevant features like tumor margins or edema delineation. Second, downstream tasks such as lesion visualization, segmentation, and lesion-level analysis, were not conducted in this work, and the framework's current validation lacks assessment of real-world variability across scanner vendors, field strengths (1.5T vs. 3T), and institutional protocols. Future work will integrate uncertainty quantification for lesion boundaries and multi-center studies to address these issues.

VII. CONCLUSION

In this paper, we proposed MambaMDN, a novel dual-domain MRI reconstruction framework that synergizes K-space complementation with modality disentanglement for multi-contrast MRI reconstruction. Unlike existing methods that rely on fusion rules, our method employs a two-stage strategy: First, we leverage fully-sampled reference K-space data to complete the undersampled target K-space, generating a de-aliased initialization that preserves anatomical structures. Second, a Mamba-based modality disentanglement module progressively eliminates reference-specific features through adaptive filtering, ensuring target-specific reconstruction fidelity. Extensive experiments on public MRI datasets demonstrate that our method consistently outperforms state-of-the-art techniques in terms of both quantitative metrics and visual quality. In summary, our work provides a new perspective on integrating cross-modal priors for high-fidelity MRI reconstruction and lays a foundation for future extensions to clinically-oriented applications.

REFERENCES

- [1] Daniel K Sodickson and Warren J Manning. Simultaneous acquisition of spatial harmonics (smash): fast imaging with radiofrequency coil arrays. *Magnetic Resonance in Medicine*, 38(4):591–603, 1997.
- [2] Klaas P Pruessmann, Markus Weiger, Markus B Scheidegger, and Peter Boesiger. Sense: sensitivity encoding for fast mri. *Magnetic Resonance in Medicine*, 42(5):952–962, 1999.
- [3] David L Donoho. Compressed sensing. *IEEE Transactions on Information Theory*, 52(4):1289–1306, 2006.
- [4] Yann LeCun, Yoshua Bengio, and Geoffrey Hinton. Deep learning. *Nature*, 521(7553):436–444, 2015.
- [5] Shanshan Wang, Zhenghang Su, Leslie Ying, Xi Peng, Shun Zhu, Feng Liang, Dagan Feng, and Dong Liang. Accelerating magnetic resonance imaging via deep learning. In *ISBI*, 2016.

- [6] Chen Qin, Jo Schlemper, Jose Caballero, Anthony N Price, Joseph V Hajnal, and Daniel Rueckert. Convolutional recurrent neural networks for dynamic mr image reconstruction. *IEEE Transactions on Medical Imaging*, 38(1):280–290, 2018.
- [7] Tran Minh Quan, Thanh Nguyen-Duc, and Won-Ki Jeong. Compressed sensing mri reconstruction using a generative adversarial network with a cyclic loss. *IEEE Transactions on Medical Imaging*, 37(6):1488–1497, 2018.
- [8] Chun-Mei Feng, Yunlu Yan, Huazhu Fu, Li Chen, and Yong Xu. Task transformer network for joint mri reconstruction and super-resolution. In *MICCAI*, 2021.
- [9] Jiahao Huang, Yingying Fang, Yinzhe Wu, Huanjun Wu, Zhifan Gao, Yang Li, Javier Del Ser, Jun Xia, and Guang Yang. Swin transformer for fast mri. *Neurocomputing*, 493:281–304, 2022.
- [10] Taejoon Eo, Yohan Jun, Taeseong Kim, Jinseong Jang, Ho-Joon Lee, and Dosik Hwang. Kiki-net: cross-domain convolutional neural networks for reconstructing undersampled magnetic resonance images. *Magnetic Resonance in Medicine*, 80(5):2188–2201, 2018.
- [11] Roberto Souza, R Marc Lebel, and Richard Frayne. A hybrid, dual domain, cascade of convolutional neural networks for magnetic resonance image reconstruction. In *MIDL*, 2019.
- [12] Shanshan Wang, Ziwen Ke, Huitao Cheng, Sen Jia, Leslie Ying, Hairong Zheng, and Dong Liang. Dimension: dynamic mr imaging with both k-space and spatial prior knowledge obtained via multi-supervised network training. *NMR in Biomedicine*, 35(4):e4131, 2022.
- [13] Zhijie Wang, Aiping Liu, Jinbao Wei, Qingguo Xie, Kongqiao Wang, and Xun Chen. Ddc-net: Dual-domain cascaded network with pocs prior for fast mri reconstruction. *IEEE Sensors Journal*, 24(7):10944–10956, 2024.
- [14] Weiyi Lyu, Xinming Fang, Chaoyan Huang, Minhua Lu, Jun Wang, Jun Shi, and Juncheng Li. Fast mri reconstruction: A thorough survey from single-modal to multi-modal. *Expert Systems with Applications*, 283:127703, 2025.
- [15] Joop J Van Vaals, Marijn E Brummer, W Thomas Dixon, Hans H Tuithof, Hans Engels, Rendon C Nelson, Brigid M Gerety, Judith L Chezmar, and Jacques A Den Boer. “keyhole” method for accelerating imaging of contrast agent uptake. *Journal of Magnetic Resonance Imaging*, 3(4):671–675, 1993.
- [16] Albert Gu and Tri Dao. Mamba: Linear-time sequence modeling with selective state spaces. *arXiv preprint arXiv:2312.00752*, 2023.
- [17] Guangyuan Li, Jun Lv, Xiangrong Tong, Chengyan Wang, and Guang Yang. High-resolution pelvic mri reconstruction using a generative adversarial network with attention and cyclic loss. *IEEE Access*, 9:105951–105964, 2021.
- [18] Bangjun Li, Weifeng Hu, Chun-Mei Feng, Yujun Li, Zhi Liu, and Yong Xu. Multi-contrast complementary learning for accelerated mr imaging. *IEEE Journal of Biomedical and Health Informatics*, 28(3):1436–1447, 2023.
- [19] Hanhui Yang, Juncheng Li, Lok Ming Lui, Shihui Ying, Jun Shi, and Tiejong Zeng. Fast mri reconstruction via edge attention. *arXiv preprint arXiv:2304.11400*, 2023.
- [20] Faming Fang, Le Hu, Jinhao Liu, Qiaosi Yi, Tiejong Zeng, and Guixu Zhang. Hfgn: High-frequency residual feature guided network for fast mri reconstruction. *Pattern Recognition*, 156:110801, 2024.
- [21] Berkin Bilgic, Vivek K Goyal, and Elfar Adalsteinsson. Multi-contrast reconstruction with bayesian compressed sensing. *Magnetic resonance in medicine*, 66(6):1601–1615, 2011.
- [22] Junzhou Huang, Chen Chen, and Leon Axel. Fast multi-contrast mri reconstruction. In *MICCAI*, 2012.
- [23] Lei Xiang, Yong Chen, Weitang Chang, Yiqiang Zhan, Weili Lin, Qian Wang, and Dinggang Shen. Ultra-fast t2-weighted mr reconstruction using complementary t1-weighted information. In *MICCAI*, 2018.
- [24] Xiuyun Zhou and Hongwei Du. A 3d multi-modal network for mri fast reconstruction. In *EIECT*, 2023.
- [25] Xuanmin Chen, Liyan Ma, Shihui Ying, Dinggang Shen, and Tiejong Zeng. Fefa: Frequency enhanced multi-modal mri reconstruction with deep feature alignment. *IEEE Journal of Biomedical and Health Informatics*, 28(11):6751–6763, 2024.
- [26] Antonio Falvo, Danilo Comminiello, Simone Scardapane, Michele Scarpiniti, and Aurelio Uncini. A wide multimodal dense u-net for fast magnetic resonance imaging. In *EUSIPCO*, 2021.
- [27] Xuebin Sun, Yanwei Pang, Yiming Liu, Caifeng Shan, and Shing Shin Cheng. Multi-modal multi-slice cooperative dual-domain cascaded de-aliasing network for mr imaging reconstruction. *IEEE Journal of Biomedical and Health Informatics*, 28(9):5370–5382, 2024.

- [28] Pengcheng Lei, Faming Fang, Guixu Zhang, and Tiejong Zeng. Decomposition-based variational network for multi-contrast mri super-resolution and reconstruction. In *ICCV*, 2023.
- [29] Jiacheng Chen, Fei Wu, and Jianwei Zheng. Multi-contrast mri reconstruction via information-growth holistic unfolding network. *IEEE Transactions on Instrumentation and Measurement*, 73:1–12, 2024.
- [30] Pengcheng Lei, Le Hu, Faming Fang, and Guixu Zhang. Joint under-sampling pattern and dual-domain reconstruction for accelerating multi-contrast mri. *IEEE Transactions on Image Processing*, 33:4686–4701, 2024.
- [31] Hongping Gan, Zitong Zhao, Yunong Chen, Shanshan Shan, Baoshun Shi, and Chunyi Liu. Apg-net: Apg optimization-induced multi-scale attention network for mri reconstruction from undersampled k-space measurements. *IEEE Transactions on Instrumentation and Measurement*, 2025.
- [32] Peng Ding, Jizhong Duan, Haibo Tao, and Yu Liu. Enhanced feature contrastive self-supervised learning method based on deep unfolding pocs for accelerated parallel mri reconstruction. *IEEE Transactions on Instrumentation and Measurement*, 2025.
- [33] Marius Arvinte, Sriram Vishwanath, Ahmed H Tewfik, and Jonathan I Tamir. Deep j-sense: Accelerated mri reconstruction via unrolled alternating optimization. In *MICCAI*, 2021.
- [34] Chong Wang, Lanqing Guo, Yufei Wang, Hao Cheng, Yi Yu, and Bihan Wen. Progressive divide-and-conquer via subsampling decomposition for accelerated mri. In *CVPR*, 2024.
- [35] Maosong Ran, Wenjun Xia, Yongqiang Huang, Zexin Lu, Peng Bao, Yan Liu, Huaiqiang Sun, Jiliu Zhou, and Yi Zhang. Md-recon-net: a parallel dual-domain convolutional neural network for compressed sensing mri. *IEEE Transactions on Radiation and Plasma Medical Sciences*, 5(1):120–135, 2020.
- [36] Jiawei Jiang, Jie Wu, Yueqian Quan, Jiacheng Chen, and Jianwei Zheng. Memory-augmented dual-domain unfolding network for mri reconstruction. In *ICASSP*, 2024.
- [37] Yue Liu, Yunjie Tian, Yuzhong Zhao, Hongtian Yu, Lingxi Xie, Yaowei Wang, Qixiang Ye, Jianbin Jiao, and Yunfan Liu. Vmamba: Visual state space model. *Advances in Neural Information Processing Systems*, 37:103031–103063, 2024.
- [38] Jiahao Huang, Liutao Yang, Fanwen Wang, Yinzhe Wu, Yang Nan, Weiwen Wu, Chengyan Wang, Kuangyu Shi, Angelica I Aviles-Rivero, Carola-Bibiane Schönlieb, et al. Enhancing global sensitivity and uncertainty quantification in medical image reconstruction with monte carlo arbitrary-masked mamba. *Medical Image Analysis*, 99:103334, 2025.
- [39] Jiahao Huang, Liutao Yang, Fanwen Wang, Yang Nan, Angelica I Aviles-Rivero, Carola-Bibiane Schönlieb, Daoqiang Zhang, and Guang Yang. Mambamir: An arbitrary-masked mamba for joint medical image reconstruction and uncertainty estimation. *arXiv preprint arXiv:2402.18451*, 2024.
- [40] Yilmaz Korkmaz and Vishal M Patel. Mambarecon: Mri reconstruction with structured state space models. In *WACV*, 2025.
- [41] Zexin Ji, Beiji Zou, Xiaoyan Kui, Pierre Vera, and Su Ruan. Deform-mamba network for mri super-resolution. In *MICCAI*, 2024.
- [42] Yucong Meng, Zhiwei Yang, Zhijian Song, and Yonghong Shi. Dm-mamba: Dual-domain multi-scale mamba for mri reconstruction. *arXiv preprint arXiv:2501.08163*, 2025.
- [43] Bjoern H Menze, Andras Jakab, Stefan Bauer, Jayashree Kalpathy-Cramer, Keyvan Farahani, Justin Kirby, Yuliya Burren, Nicole Porz, Johannes Slotboom, Roland Wiest, et al. The multimodal brain tumor image segmentation benchmark (brats). *IEEE Transactions on Medical Imaging*, 34(10):1993–2024, 2014.
- [44] Mengye Lyu, Lifeng Mei, Shoujin Huang, Sixing Liu, Yi Li, Kexin Yang, Yilong Liu, Yu Dong, Linzheng Dong, and Ed X Wu. M4raw: A multi-contrast, multi-repetition, multi-channel mri k-space dataset for low-field mri research. *Scientific Data*, 10(1):264, 2023.
- [45] Olaf Ronneberger, Philipp Fischer, and Thomas Brox. U-net: Convolutional networks for biomedical image segmentation. In *MICCAI*, 2015.
- [46] Syed Waqas Zamir, Aditya Arora, Salman Khan, Munawar Hayat, Fahad Shahbaz Khan, and Ming-Hsuan Yang. Restormer: Efficient transformer for high-resolution image restoration. In *CVPR*, 2022.
- [47] Xuanhua He, Ke Cao, Jie Zhang, Keyu Yan, Yingying Wang, Rui Li, Chengjun Xie, Danfeng Hong, and Man Zhou. Pan-mamba: Effective pan-sharpening with state space model. *Information Fusion*, 115:102779, 2025.
- [48] Jing Zou, Lanqing Liu, Qi Chen, Shujun Wang, Zhanli Hu, Xiaohan Xing, and Jing Qin. Mmr-mamba: Multi-modal mri reconstruction with mamba and spatial-frequency information fusion. *Medical Image Analysis*, 102:103549, 2025.
- [49] Ze Liu, Yutong Lin, Yue Cao, Han Hu, Yixuan Wei, Zheng Zhang, Stephen Lin, and Baining Guo. Swin transformer: Hierarchical vision transformer using shifted windows. In *ICCV*, 2021.